The air flow around a milling cutter investigated experimentally by particle image velocimetry

Cite as: AIP Conference Proceedings **2323**, 030006 (2021); https://doi.org/10.1063/5.0041860
Published Online: 08 March 2021

Tereza Kubíková

The Air Flow around a Milling Cutter Investigated Experimentally by Particle Image Velocimetry

Tereza Kubíková[a)]

Department of Power System Engineering, Faculty of Mechanical Engineering, University of West Bohemia in Pilsen, Univerzitní 22, 306 14, Pilsen, Czech Republic.

[a)]Corresponding author: kubice-ter@seznam.cz

Abstract. The movement of air around a rotating milling cutter is investigated experimentally by using the optical non-intrusive method PIV (Particle Image Velocimetry). The milling cutter is located next to a flat surface simulating the processed material. The Flow is studied in three planes in axial × radial direction with phases 90°, 180° and 270° from the point closest to the flat desk. The PIV timing has been synchronized with the cutter rotation. We observed plumes governed by centrifugal force (as in Taylor-Couette flow) acting on the air teared with the rotating milling cutter. In average, the air flows along the milling cutter from its front end forming a large-scale vortex mostly apparent at higher velocity and at the plane opposite to the processed surface. At the 90°plane, the air is sucked towards the milling cutter, while at the 270°plane, the air is pushed away from it. Spatial correlation function shows a weak periodicity close to the cutter and widening of its shape with increasing distance from the milling cutter.

INTRODUCTION

The general problem of flow around a rotating cylinder is known under the term *Taylor-Couette flow* [1, 2], where the Taylor instability [3, 4] exerts. This instability relates with the more generalized Rayleigh type of instabilities, where two volumes of fluid are forced in opposite direction. In the rotating case, such a role is played by the centrifugal force, which pushes the fluid, which is closer to the rotating object, against that fluid, which is more far and thus less rotating. The Kelvin-Helmholtz instability [5] occurs at the shear layers of fluid volumes moving by different velocities, and it can be observed e.g. in a jet [6, 7] or in a wake [8]. A similar mechanism causes the secondary flow of second kind in [9, 10], but not in the case of so called *steady streaming* [11]. The most spectacular example of Rayleigh instability is the Rayleigh-Bénard instability leading to thermal convection [12, 13]. Similar to the rotating case, this type of convection is characterized by the presence of *plumes* – a mushroom like vortex ring followed by a spike. This coherent structure is not universal for thermal convection as, in superfluids, the heat transfer is realized via the *thermal counterflow* [14, 15] of normal and superfluid component flowing one through the other in opposite direction. In both systems – the classical one and the quantum one, the developed turbulence displays universal features [16], although its microscopic nature is as different as possible [17]. The similarity of classical and quantum turbulence on large scales is demonstrated by the existence of wakes [18], secondary flows [11] or cavitation bubbles [19] in both systems.

One of the most practical effect of turbulence is the enhancement of mixing, as the mixing occurs at all scales from the largest one in the system (called integral length-scale) down to the smallest one, where the energy dissipates (called Kolmogorov scale). This has a large impact on the heat transfer from the hot object (which is in our case the milling cutter) into the surroundings. Therefore, the investigation of the structures and scales of turbulence around this device during its job can help us to understand the heat transfer needed for effective cooling.

19th Conference on Power System Engineering
AIP Conf. Proc. 2323, 030006-1–030006-8; https://doi.org/10.1063/5.0041860
Published by AIP Publishing. 978-0-7354-4067-8/$30.00

EXPERIMENTAL SETUP

The milling cutter with 5 blades is situated on a flat plate simulating the processed object as sketched in Fig. 1. By using the ATOS 3D optical scanner, we measured the milling cutter major diameter to be 25.3 mm, while the minor one to be 15.1 mm, the active length to be 65 mm and the pitch to be 22.6 mm (note there are 5 blades, thus one blade twists ones in 113 mm). The flow is investigated in three planes with phase shifts from the point closest to the solid surface are 90°, 180° and 270°. The side size of the planes is 75 mm.

The milling cutter is powered by using a drill, which offers only two stable rotation speeds: the slower one is measured to be 7.72 Hz, while the faster one 19.7 Hz.

We use the Particle Image Velocimetry technique, which measures optically the motion of small particles (droplets of oil) carried by the fluid and illuminated by a laser sheet. We use a commercial system from the company Dantec with Mk II Flow Sense camera and New Wave Solo solid state laser. The tracking particles are produced by a fog generator Safex. The maximum frequency of the PIV system is 7.4 Hz, thus we are not able to detect the time evolution. Our data have character of an ensemble of statistically independent snapshots.

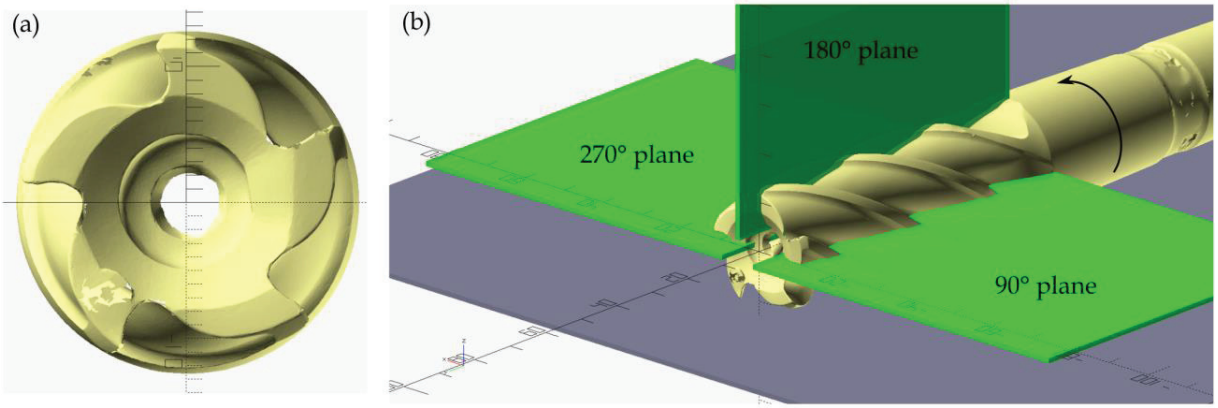

FIGURE 1. (a) 3D scan of the used milling cutter. Front view. It rotates in counterclockwise direction. (b) 3D scan situated together with the planes studied by using the PIV method (depicted as a green transparent planes), the dark plane bellow represents the solid surface simulating the processed object, although there is not touch between them in the current setup.

The timing of the PIV system (the laser shots and the camera exposure) are synchronized with the rotation of the milling cutter by using a custom made electrical circuit based on the Arduino microcontroller, which triggers the signal from a photodiode placed next to the rotating shaft with a small reflective strip.

We use PIV in configuration with a single camera, thus only the in-plane velocity components can be measured. In the later we refer to the axial velocity component as u and the radial as v, the tangential one is not measured, although it can be energetically dominant. This has to be taken into account when interpreting the results.

In order to prevent unwanted reflections of the laser beam, the milling cutter has been painted to black. Other optical disturbances have been suppressed by subtracting the spatial map of minimal point intensities. The milling cutter was masked out in order to prevent spurious velocity vectors in the area, where cannot be any particles. Standard method “Adaptive PIV” in Dantec Dynamic Studio software has been used to calculate the velocity vectors from the captured images. The ensemble of such velocity fields was filtered by the energy of small-scale fluctuations. The last method has been developed by my great supervisor and published in article [7].

OBSERVATIONS

Plumes in Instantaneous Velocity Field

The instantaneous velocity fields often display one of the feature typical for all Rayleigh-type instabilities. This esthetic flow pattern is called *plume* and few examples of them is shown in Fig. 2. We show the plumes in the 90° plane (Fig. 2), because the plumes there are on the start of their development and thus are not yet turbulized and mixed, as it is apparent in the 180° plane (Fig. 3).

The vorticity displayed in Fig. 2 and 3 is calculated from the instantaneous velocity as

$$\omega = \nabla \vec{u} \tag{1}$$

where instead of the differential operator nabla (∇) we used the symmetric differentiation on the grid of spatial resolution $\Delta x, \Delta y$, thus

$$\omega(x,y) = \frac{u(x,y+\Delta y) - u(x,y-\Delta y)}{2\Delta y} - \frac{v(x+\Delta x,y) - v(x-\Delta x,y)}{2\Delta x} \tag{2}$$

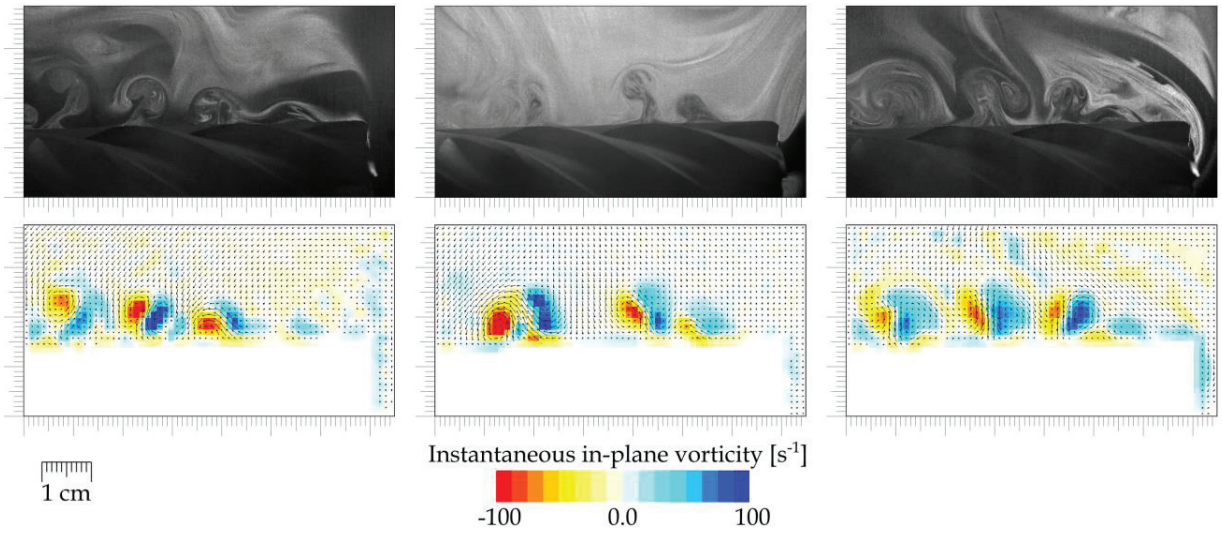

FIGURE 2. Top row shows a few typical images taken during the experiment and the bottom row shows velocity vectors obtained from the images above and colored by the instantaneous in-plane vorticity (color version online). All data are taken at the slower rotational speed in the 90° plane (see Fig. 1 for reference).

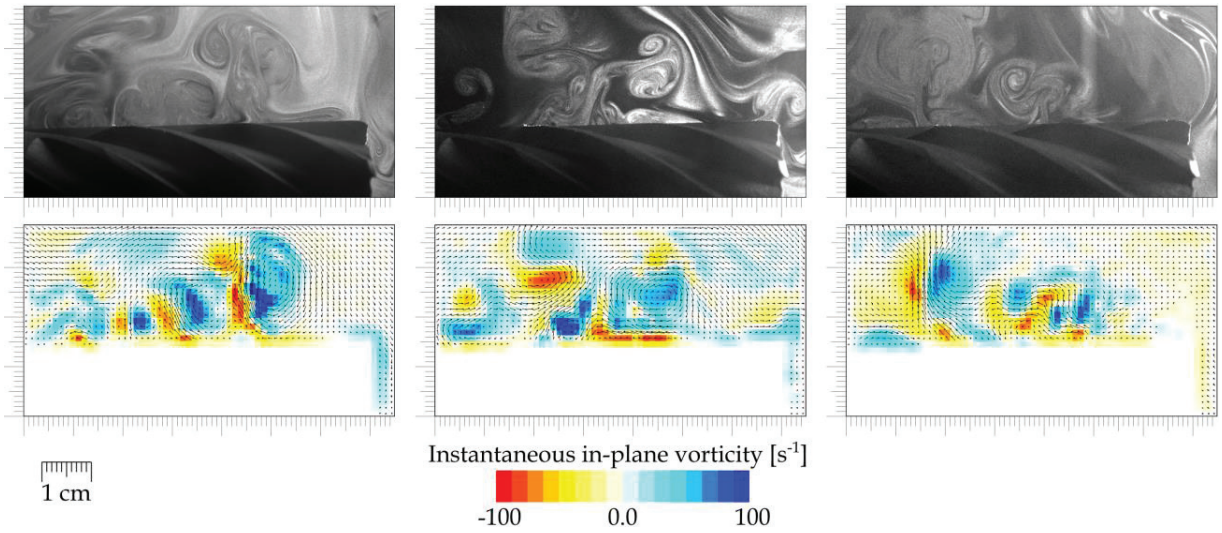

FIGURE 3. Plumes in raw images (top row) and the vorticity (bottom row) observed in the 180° plane at the slower rotational speed.

Plume is a part of fluid, which is moved through its surrounding due to some force acting to it and not (or less) to the surroundings. They are typically observed in the system of thermal convection, especially, when the heat source is localized, as it is e.g. in the case of an explosion ("nuclear mushroom"). In the rotating system, the leading force is the centrifugal force acting more strongly to the fluid, which share rotational motion with the milling cutter.

Average Velocity Fields

The spatial distribution of ensemble-average velocity is shown in Fig. 4. We can see, that first the air flows towards the milling cutter, there are still observable some middle-scale vortices close to the rotating cutter. Later, the flow pattern is dominated by a large-scale vortex at the middle of the milling cutter length and, at the phase before the processed surface, the air leaves the area rotating with the body, but middle-scale average structures are apparent. Close to the body, the flow is pushed along the axis (from right to left in the figures) due to the helicity of the milling cutter. This is the reason, why there is low turbulence intensity at the milling cutter tip (see turbulent kinetic energy in Fig. 6 and 7) – there is sucked the air from quiet surroundings.

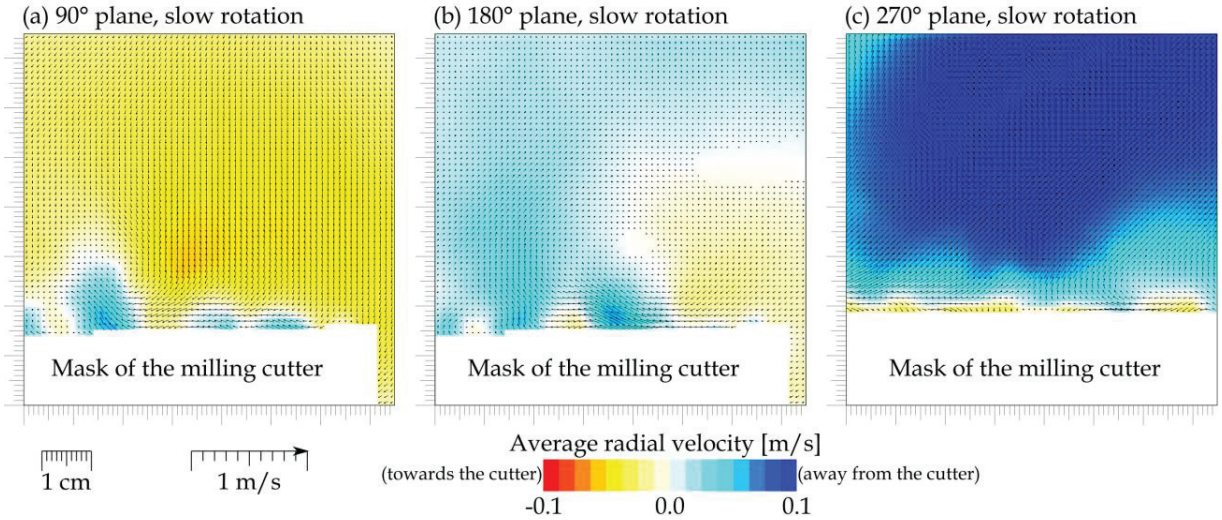

FIGURE 4. Average velocity displayed as vectors, color corresponds to its radial component (color version online). The panels (a), (b) and (c) show planes in different phase position around the rotating thing, see Fig. 1 for reference. The mask is little bit larger than the milling cutter in order to cover the unwanted laser reflections, which causes troubles especially at the 270° plane.

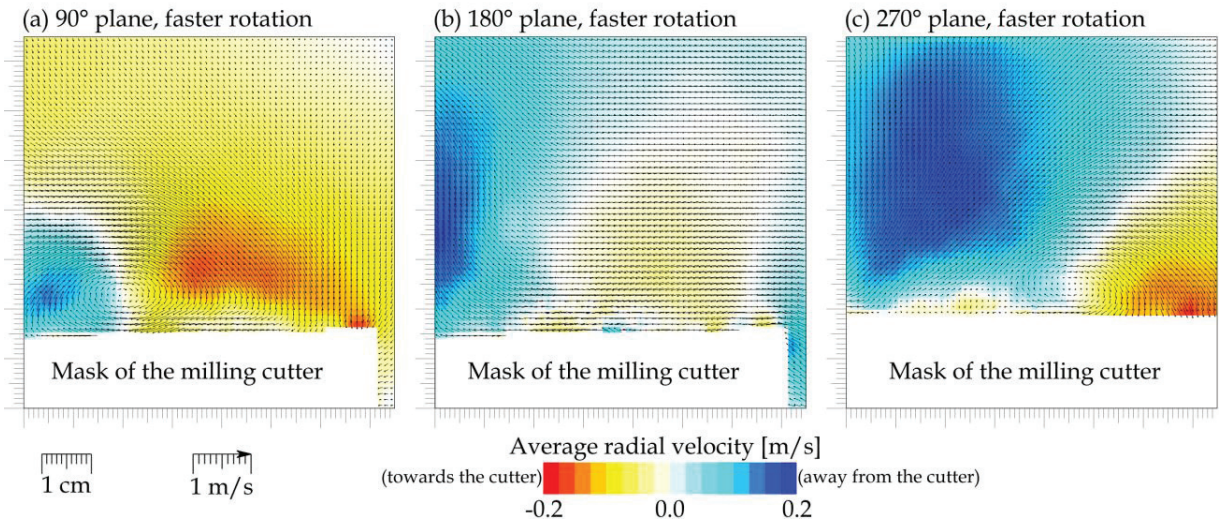

FIGURE 5. Average velocity under the faster studied rotational speed, color corresponds to the radial component of average velocity (color version online).

The average behavior of the flow is quite different under the faster rotational speed: first note, that the large vortex (formed in the 180° plane at the slower rotation) is apparent since the first 90° plane. At the 180° plane, this vortex is

so large, it is barely visible, the outcoming region is shifted along the milling cutter axis behind the active length (left edge of the Fig. 5), while the sucking region covers more than half of the active length. The scheme of sucking and pushing the fluid at different planes is now represented solely by shift in the position of the main vortex, therefore the overall flow in the 90° is towards the milling cutter, while at 270° it goes away from it. The middle scale structures visible at slower velocity (Fig. 4) are covered by the dominant vortex, but their presence will be shown in next section.

Figures 6 and 7 shows the spatial distribution of the turbulent kinetic energy (TKE). TKE is calculated as the sum of variances of the velocity component ensembles in each point:

$$k = \frac{1}{2}(\langle u^2 \rangle - \langle u \rangle^2) + \frac{1}{2}(\langle v^2 \rangle - \langle v \rangle^2) \tag{3}$$

where $\langle \cdot \rangle$ is the ensemble averaging. TKE is displayed preferentially than the intensity of turbulence, as the intensity of turbulence can diverge in the areas of low average velocity. Naturally, TKE in our case is calculated only by using the measured velocity components, i.e. the axial one (u) and the radial one (v), although the third (tangential) component might be expected to dominate this flow problem.

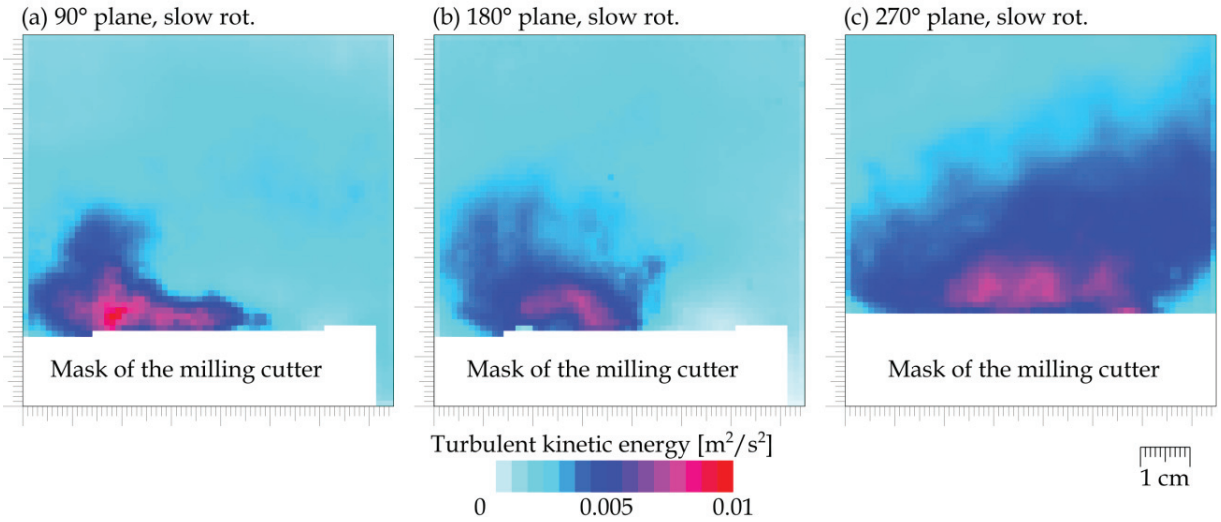

FIGURE 6. Turbulent kinetic energy calculated from the in-plane velocities and its fluctuations. Note that this TKE is computed by using only the in-plane velocity fluctuations. Color version online.

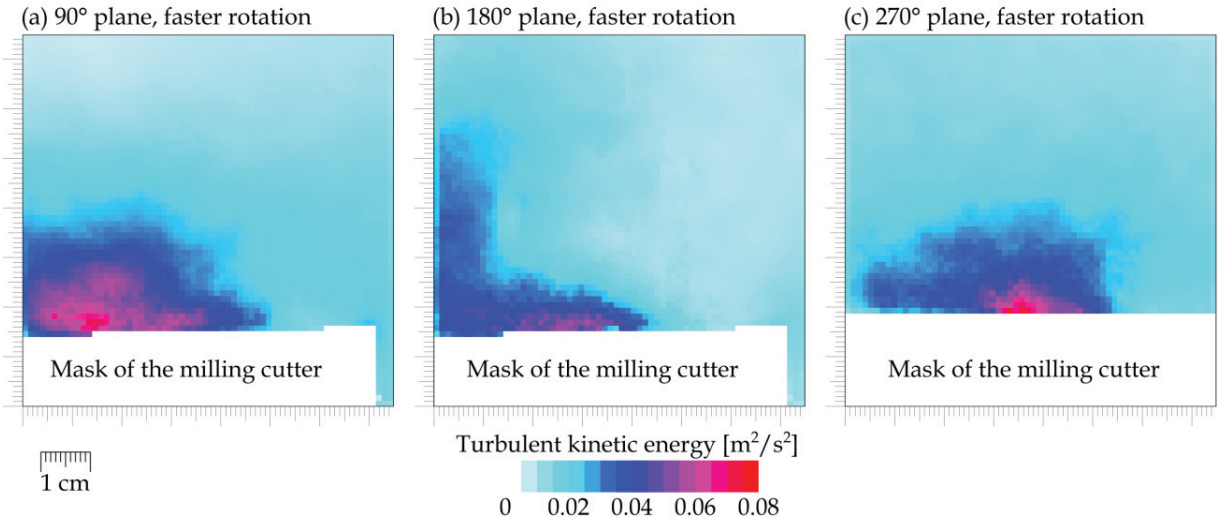

FIGURE 7. Turbulent kinetic energy at the faster rotational speed. Color version online.

Length-scale of the Fluctuations

The length-scale of fluctuations is characterized by the correlation function R_{vv} of two quantities, in this case we choose as the relevant quantity the radial component of velocity. R_{vv} in the spatially resolved data is defined as

$$R_{vv}(\Delta x, \Delta y) = \frac{\langle \big(v(x,y) - V(x,y)\big) \cdot \Big(\big(v(x+\Delta x, y+\Delta y) - V(x+\Delta x, y+\Delta y)\big)\Big)\rangle_T}{\sigma[v(x,y)] \cdot \sigma[v(x+\Delta x, y+\Delta y)]} \tag{4}$$

where σ represents the standard deviation, V is the ensemble average at the current point, thus the difference $v(x,y) - V(x,y)$ is the *Reynolds decomposition.* Note that the correlation function makes sense only when applied to the Reynolds decomposed velocity fields, otherwise it does not converge. The value of correlation coefficient reaches the values from -1 to 1, where 1 means, that the two points are statistically same, while -1 means, they are opposite. 0 is usually interpreted as a statistical independency, but it can also signify a phase shift by $\pi/2$ (imagine the correlation function of $\sin x$ and $\cos x$ – it is identically 0, although both are functions of the same variable and thus depends one on the other). Nothing to say, that the correlation function inherits some properties of the original function, among others its periodicity.

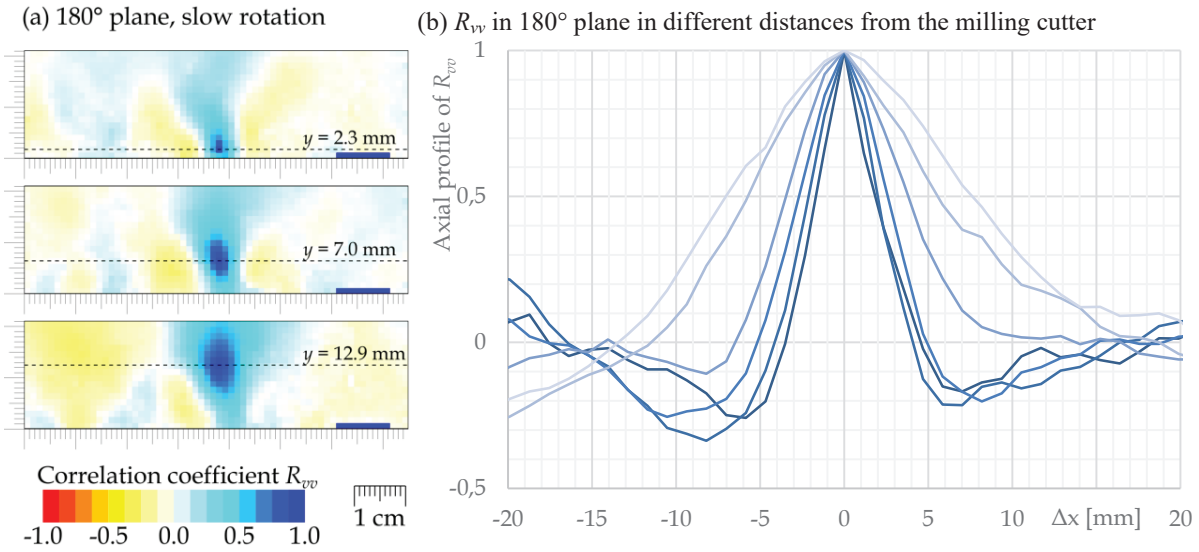

FIGURE 8. Correlation coefficient R_{vv} of the fluctuation of radial velocity component v in the 180° plane at the slower rotational speed. (a) the spatial distribution of R_{vv} with point at different radial distance from the milling cutter. The milling cutter is located under the bottom edge of that crops. (b) the profiles of R_{vv} along the axial direction; different lines represent different radial distance from the milling cutter starting from the 1.17 mm (darkest color) to 18.7 mm (clearest color).

In turbulence research, the correlation function is often used to determine a size of the fluctuation, i.e. a distance, where fluctuations disappear. Figure 8 shows how the correlation function of radial velocity fluctuations depends on the distance from the milling cutter. At closer distance, we see a periodicity (R_{vv} reaches negative values and then returns to around 0) of length about 6 – 8 mm, later this behavior disappears and the correlation function widens as the fluctuations are larger. The slope of the R_{vv} close to zero is theoretically zero as the fluid motion at smallest scales (Kolmogorov scales) is smoothed due to finite viscosity. We do not observe this feature as our spatial resolution (1.17 mm per grid point) is insufficient and this remains as an open task for future research.

When comparing the two different rotational speeds (compare Fig. 9 with Fig. 10), we see the shape of the correlation function is sharper, while the distance of reaching zero remains similar (this is probably due to the periodicity close to the milling cutter). The shape does not seem to change much among the different explored planes, it is widest in the 90° plane, where the flow is not yet developed and thus it is characterized by sucking the surrounding non-turbulized fluid and by developing laminar plumes. Surprisingly, the 270° plane, where the fluid is pulled out due to approaching the processed desk, displays little bit wider shape of the correlation function, than the 180° plane opposite to the processed surface.

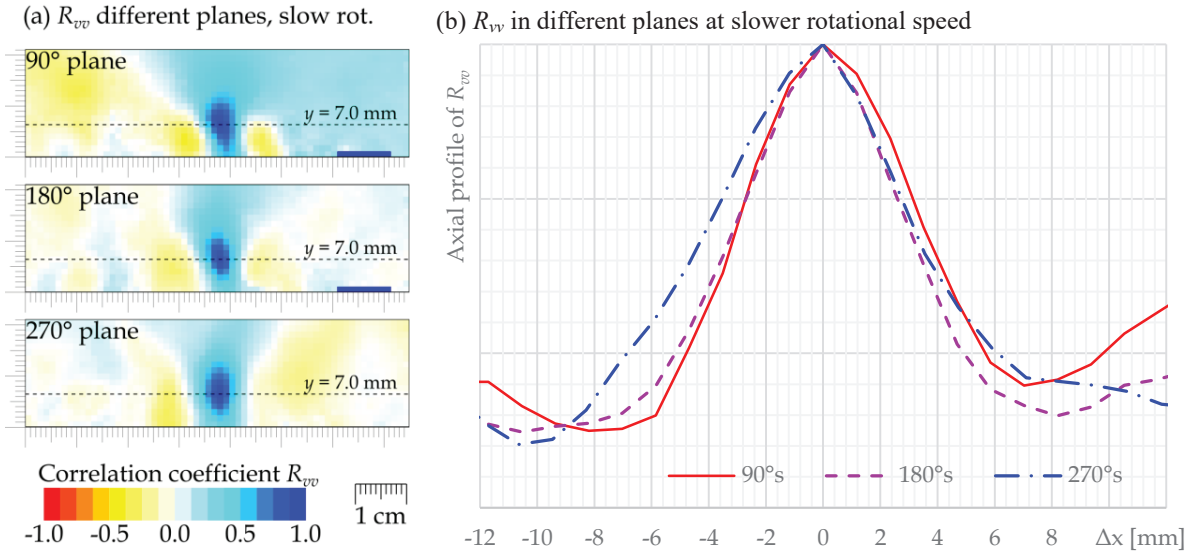

FIGURE 9. Correlation coefficient R_{vv} of the fluctuation of radial velocity component v in different planes (see Fig. 1 for reference) at the slower rotational speed. (a) the spatial distribution of R_{vv} The milling cutter is located under the bottom edge of that crops. (b) the profiles of R_{vv} along the axial direction. (Color version online)

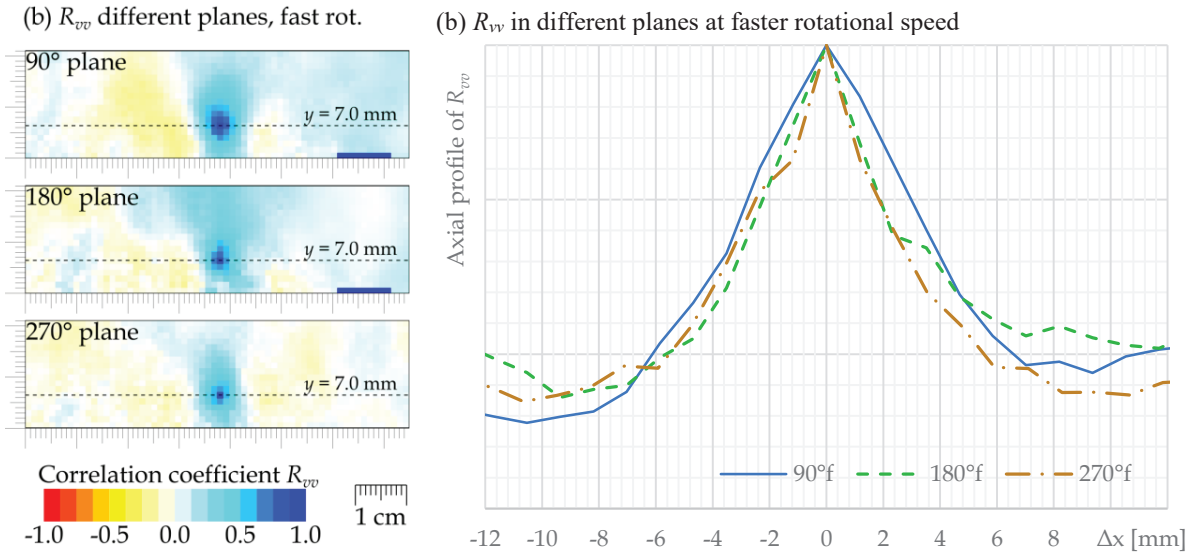

FIGURE 10. Correlation coefficient R_{vv} of the fluctuation of radial velocity component v in different planes (see Fig. 1 for reference) at the faster rotational speed. (a) the spatial distribution of R_{vv} The milling cutter is located under the bottom edge of that crops. (b) the profiles of R_{vv} along the axial direction. (Color version online)

CONCLUSION

The flow around a rotating milling cutter has been investigated experimentally by using the Particle Image Velocimetry (PIV) technique in three planes and at two rotational speeds. The planes were oriented in axial × radial direction covering the entire active length of the milling cutter (which is 65 mm). The planes have been situated in three different phases from the touching point with the processed surface (the surface is not milled in this experiment). The investigated phases were 90°, 180° and 270°. Only the axial and radial in-plane velocity components have been measured

The flow was teared together with the rotating body, therefore it felt the centrifugal force similarly as in the Taylor-Couette problem, which has been proven by the observation of plumes carrying the faster rotating fluid outside into the slower fluid. In the average, the flow has formed a large-scale vortex sucking the air at the open end of the milling cutter, pulling it in axial direction and pushing away at the shaft end. This vortex was stronger under the faster rotation. In the 90° plane, the air is sucked towards the rotating milling cutter, while in the 270° we observed the air flowed away from it. This effect had a form homogeneous motion under the slower rotation, while under the faster one, it just moved the center of the just mentioned large-scale vortex.

Spatial correlation function of radial velocity component has shown a weak periodicity close to the cutter, which disappeared in distances larger than 1 cm. The shape of correlation function peak widened with increasing distance from the milling cutter. Larger rotational speed leaded to narrowing that peak, while the base width remains similar.

ACKNOWLEDGMENTS

This work was financially supported by student project SGS-2019-021 (Improving the efficiency, reliability and service life of power machines and equipment 5). I thank to my supervisor RNDr. Daniel Duda, Ph.D. for significant help with data analysis and article writing. I thank to doc. Vitalii Yanovych, DrSc. for technical help and to prof. Ing. Václav Uruba, CSc. for discussions.

REFERENCES

1. C. D. Andereck, S. S. Liu and H. L. Swinney, J. Fluid Mech. **164**, 155-183 (1986)
2. W. W. Saric, Annu. Rev. Fluid Mech. **26**, 379-409 (1994)
3. M. A. Fardin, C. Perge and N. Taberlet, Soft Matter **10**, 3523-3535 (2014)
4. D. Duda, M. Klimko, R. Škach, J. Uher and V. Uruba, EPJ Web of Conf. **213**, 02014 (2019)
5. G.E. Volovik, JETP Letters **75**, 418-422 (2002)
6. D. Duda, AIP Conf. Proc. **2047**, 020001 (2018)
7. D. Duda and V. Uruba, ASME J of Nuclear Rad Sci **5**(3), 030912 (2019)
8. D. Duda and V. Uruba, AIP Conf. Proc. **2000**, 020005 (2018)
9. M. Uhlmann, A- Pinelli, G. Kawahara and T. Sekimoto, J. Fluid Mech. **588**, 153-162 (2007)
10. D. Duda, J. Bém, V. Yanovych, P. Pavlíček and V. Uruba, Eur. J. Mech. B Fluids **79**, 444-453 (2020)
11. D. Duda, M. La Mantia and L. Skrbek, Phys. Rev. B **96**, 2, 024519 (2017)
12. P. Urban, V. Musilová and L. Skrbek, Phys. Rev. Lett. **107**, 014302 (2011)
13. P. Urban, P. Hanzelka, I. Vlček, D. Schmoranzer and L. Skrbek, Low Temp. Phys. **44**, 1001-1004 (2018)
14. D. Duda, M. La Mantia, M. Rotter and L. Skrbek, J. Low Temp. Phys **175**, 331-338 (2014)
15. M. La Mantia, D. Duda, M. Rotter and L. Skrbek, J. Fluid Mech **717**, R9 (2013)
16. M. La Mantia, P. Švančara, D. Duda and L. Skrbek, Phys. Rev. B **94**, 18, 184512 (2016)
17. C. F. Barenghi, V. S. L'vov, and P. E. Roche, P. Natl. Acad. Sci. USA, **111**:4683-4690 (2014)
18. D. Duda, P. Švančara, M. La Mantia, M. Rotter and L. Skrbek, Phys. Rev. B **92**, 064519 (2015)
19. D. Duda, P. Švančara, M. La Mantia, M. Rotter, D. Schmoranzer, O. Kolosov and L. Skrbek, J Low Temp. Phys. **187**, 5-6, 376-382 (2017)